Supplementary materials

Photocatalytic degradation of Rhodamine-B by visible light assisted peroxymonosulfate activation using Z-scheme MIL-100(Fe)/Bi_2S_3 composite: a combined experimental and theoretical approach

Debashis Roy[a], Niladri Poddar[b], Manmohanpreet Singh[a], Sudarsan Neogi[a], Sirshendu De[a]*

a. Department of Chemical Engineering, Indian Institute of Technology Kharagpur, Kharagpur – 721302, India

b. Department of Chemical Engineering, Heritage Institute of Technology, Kolkata – 700107, India

* Corresponding author

Tel: 91-3222-283926

Fax: 91-3222-255303

E-mail – sde@che.iitkgp.ac.in

S1. Experimental section

S1.1. Materials required

Bismuth nitrate pentahydrate ($Bi(NO_3)_2$, $5H_2O$, MW: 395.0 g/mol), Ferric chloride hexahydrate ($FeCl_3$, $6H_2O$, MW: 270.3 g/mol), Thiourea (CH_4N_2S, MW: 76.12 g/mol), Rhodamine B (RhB, $C_{28}H_{31}Cl\ N_2O_3$, MW: 479.02 g/mol), Oxone (Potassium peroxymonosulfate, PMS, $2KHSO_5$, $KHSO_4$, K_2SO_4, MW: 307.38 g/mol), Triethyl amine (TEA, $(C_2H_5)_3N$, MW: 101.19 g/mol), Tert-butyl alcohol (TBA, $(CH_3)_3COH$, MW: 74.12 g/mol), L-histidine (His, MW: 155.56 g/mol), p-Benzoquinone (pBQ, MW: 108.09 g/mol), Sodium chloride (NaCl, MW: 58.5 g/mol), Sodium sulfate (Na_2SO_4, MW: 142.04 g/mol), Sodium nitrate ($NaNO_3$, MW: 85 g/mol), Sodium carbonate (Na_2CO_3, MW: 106 g/mol), Disodium hydrogen phosphate (Na_2HPO_4, MW:142 g/mol), Humic acid (HA, 60-70% dry basis) were purchased from M/s. Loba Chemie Pvt. Ltd., India. Methanol (CH_3OH, MW: 32.04 g/mol) was obtained from M/s. Spectrochem Pvt. Ltd., Mumbai, India. Ethylene diamine tetraacetic acid disodium salt (EDTA-2Na, MW: 372.24 g/mol) and N, N-dimethyl formamide (DMF, MW: 73.09 g/mol) were procured from M/s. Merck Life sciences Pvt. Ltd., India. 1,3,5-Benzenetricarboxylic acid (Trimesic acid, H_3BTC, $C_6H_3(COOH)_3$, MW: 210.14 g/mol) was purchased from Sigma Aldrich, USA. Deionized (DI) water (resistivity: 18.2 MΩ.cm) used in this study was obtained from a Millipore water purification system supplied by Merck (India) Pvt. Ltd. All the chemicals were of analytical grade and used without any further purification. 0.45 µm Whatman PTFE syringe filters were procured from GE healthcare, UK. All glassware used in this study were procured from Borosil glass works Pvt. Ltd., Kolkata, India.

S1.2. Characterization methods

The synthesized solid powder was analyzed using field-emission scanning electron microscopy (FESEM, model: JEM 7610F, JEOL, Japan) to determine the crystal morphology and structure. The crystallographic details of the materials was evaluated using X-ray diffraction spectroscopy (XRD, model: Panalytical Xpro, Panalytical, The Netherlands) using Cu Kα radiation (λ= 1.5418 Å) within scanning range of 1.5° to 85°. Heterojunction microstructure was analyzed using high-resolution transmission electron microscopy (HRTEM, model: JEM 2100F, JEOL, Japan). Oxidation states of the constituent elements were determined using X-ray photoelectron spectroscopy (XPS, model: PHI 5000 VERSAPROBE– II M/S. Physical

Electronics, USA). Surface chemical functionalities of the material was evaluated using Fourier transform infrared spectroscopy (FTIR, model: Analyst-100, Perkin Elmer, The Netherlands). Zeta potential of the composite in water was studied using a zetasizer instrument (model: Zetasizer nano, Malvern Instruments, UK). Porous structure of the solids was studied using a BET analyzer (model: Autosorb-1, Quantochrome Instruments, UK). Ultraviolet-visible diffuse reflectance spectroscopy (UV-Vis DRS) of the composites were analyzed using an UV-Vis spectrophotometer (model: Cray-5000, Agilent Technologies, USA). The obtained data was then converted to absorbance by the Kubelka-Munk method. RhB degradation intermediates were identified based on the molecular mass distribution determined using a MALDI-TOF/TOF instrument (model: Ultraflextreme, Bruker Daltonik GmbH Life Sciences, Germany).

S1.3. Experimental procedure

Specified amount of RhB dye powder was dissolved in measured amount of DI water to prepare stock solution having fixed initial dye concentration (1000 mg/l). For each experiment, the stock dye solution was diluted suitably using DI water to prepare solutions of lower concentrations. In a typical experimental scheme, equal volume (50 ml) of dye solution was taken in different number of Erlenmeyer flasks (250 ml capacity). In each flask, specified amount of powder catalyst was added and subsequently, the mixtures were placed in an incubator under continuous rotation (150 rpm) without any irradiation (dark condition). The mixtures were kept for 30 mins to attain the adsorption-desorption equilibrium. Then, specific amount of oxidant (PMS) was added into the system and the mixtures were kept under constant rotation and visible light irradiation (intensity: 80 W). At definite predetermined time point, specific flask was withdrawn and the solid catalyst was separated from the dye solution by passing through a 0.45-micron PTFE membrane. In a parallel experiment, the samples, after attaining the adsorption-desorption equilibrium (in dark condition) were collected to determine the extent of RhB removal through adsorption. The collected samples were analyzed immediately to determine the residual dye concentration. Similar type of kinetic experiments were performed at three different operating temperatures and different initial solution pH. Effects of various coexisting ions and organic matters were evaluated by adding various salts and humic acid into the reaction medium. Effect of initial dye concentration was studied by carrying out experiments with solutions having different initial dye concentrations. Typical scavengers were employed to determine the relative inhibitory effects on the degradation

performance of the catalyst/PMS pairs and identification of various reactive species in the medium. Finally, the used catalyst was separated through centrifugation and subsequently washed with DI water before using for subsequent experiments.

S1.4. Analytical methods

Dye concentration in the solution was measured using an UV-Vis spectrophotometer (model: Perkin Elmer, USA) and comparing with an already prepared calibration curve. Residual total organic carbon (TOC) of the samples was measured using a TOC analyzer (model: TOC-L, Shimatzu Corporation, Japan). pH of the solutions was measured using a multimeter (model: PCSTester, Eutech Instruments, Singapore). Concentration of leached metals (Fe, Bi) in the filtered solution was measured using an inductively coupled plasma emission spectroscopy, mass spectrometry instrument (model: iCAP^{TM}, Thermo Fisher Scientific, USA). Percentage removals of dyes, due to adsorption and catalytic degradation, were calculated using the formula: % adsorbed $=\left(1-\frac{C_a}{C_i}\right)\times 100$, % degraded $=\left(1-\frac{C_f}{C_a}\right)\times 100$, where, C_a, C_f and C_i are the final dye concentration after adsorption, final dye concentration after degradation and initial dye concentration, respectively.

S1.5. Regeneration procedure

After each catalytic experiment, the solid catalyst was collected through centrifugation and subsequently washed several times with DI water. Then, the washed powder was dried at 100C in a hot air oven and used in subsequent experiments. Further, for each regeneration cycle, the concentration of leached metals was determined using the procedure discussed previously.

S2. Characterization of materials

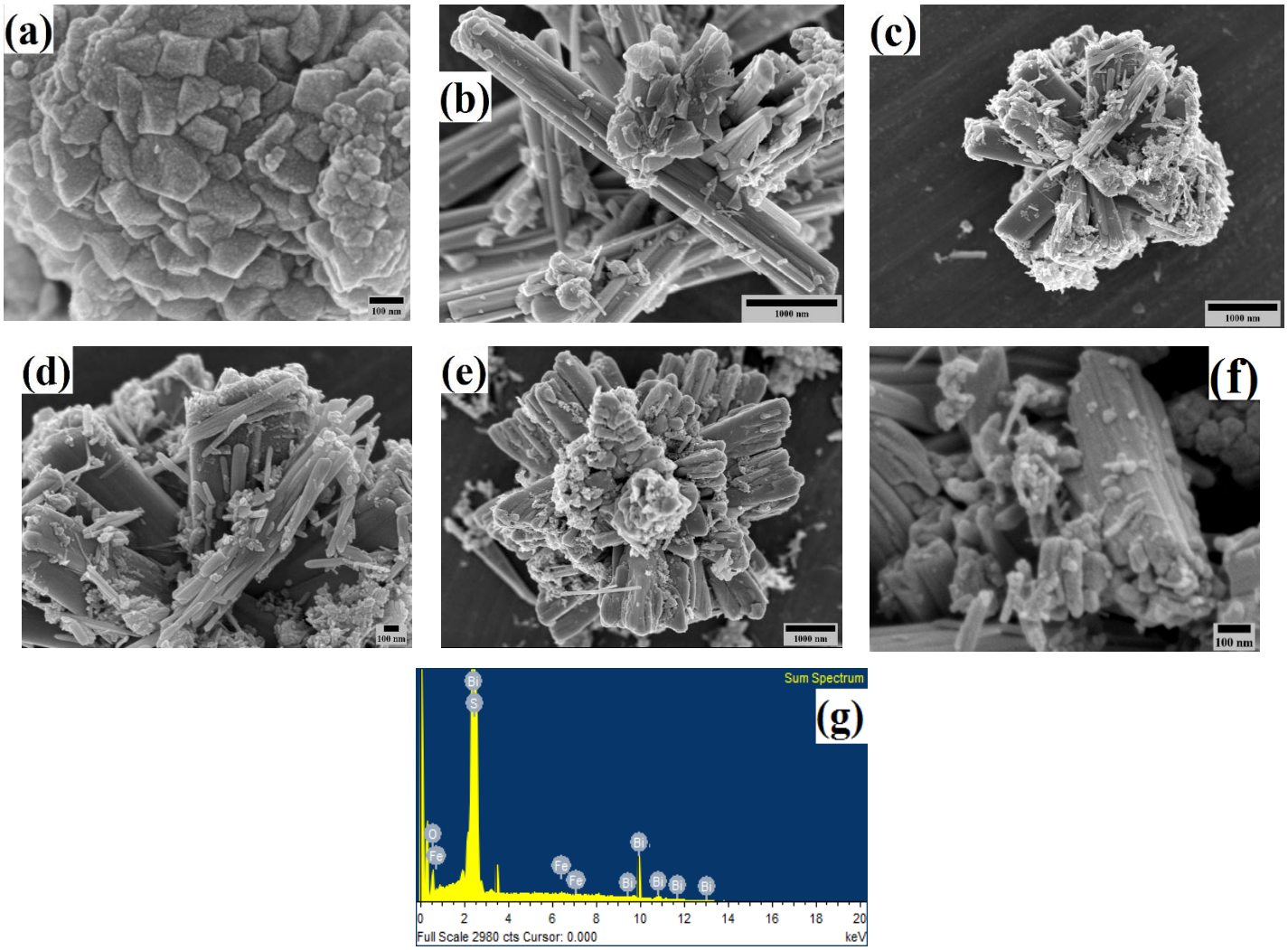

Fig. S1. SEM images of (a) unreacted MIL-100(Fe); (b,c) MIL-BS(10); (d,e,f) MIL-BS(20); (g) EDS profile of MIL-BS(10).

Table S1: Detailed elemental distribution based on EDS analysis

Elements	Binary composites							
	MIL-BS(5)		MIL-BS(10)		MIL-BS(15)		MIL-BS(20)	
	Wt%	Atomic%	Wt%	Atomic%	Wt%	Atomic%	Wt%	Atomic%
C	61.63	72.65	41.55	52.8	54.47	69.09	46.94	64.24
O	27.91	24.67	45.56	42.75	27.21	25.88	27.58	28.31
S	2.65	1.17	6.67	3.24	7.7	3.66	9.77	5.01
Fe	5.31	1.34	2.11	0.57	3.21	0.87	5.66	1.66
Bi	2.51	0.17	4.11	0.65	7.41	0.54	10.05	0.79

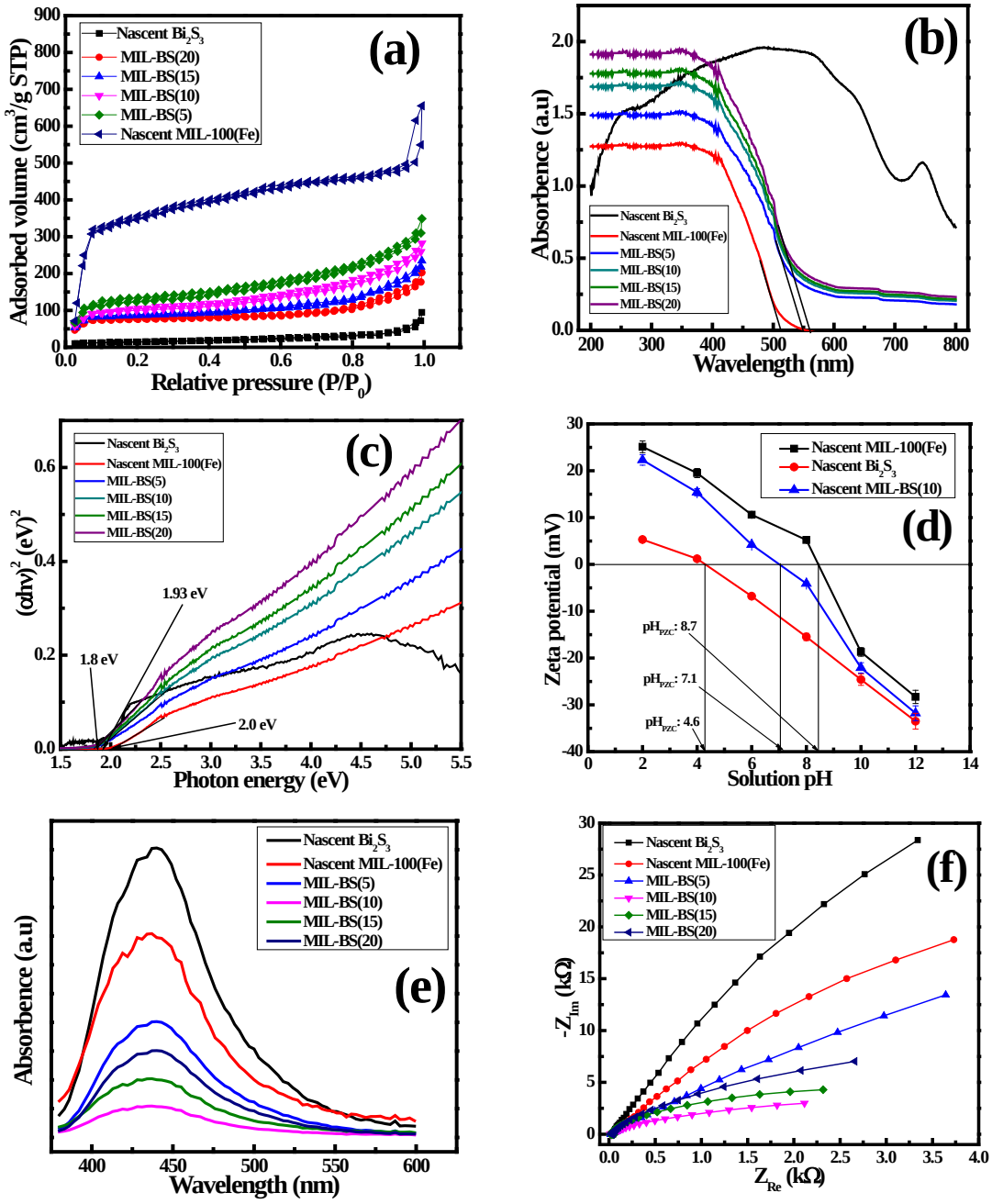
(a)
Nascent Bi_2S_3
MIL-BS(20)
MIL-BS(15)
MIL-BS(10)
MIL-BS(5)
Nascent MIL-100(Fe)
Adsorbed volume (cm^3/g STP)
Relative pressure (P/P_0)
(b)
Absorbence (a.u)
Wavelength (nm)
(c)
$(\alpha h\nu)^2$ $(eV)^2$
1.93 eV
1.8 eV
2.0 eV
Photon energy (eV)
(d)
Nascent MIL-100(Fe)
Nascent Bi_2S_3
Nascent MIL-BS(10)
Zeta potential (mV)
pH_{PZC}: 8.7
pH_{PZC}: 7.1
pH_{PZC}: 4.6
Solution pH
(e)
Absorbence (a.u)
Wavelength (nm)
(f)
$-Z_{Im}$ (kΩ)
Z_{Re} (kΩ)

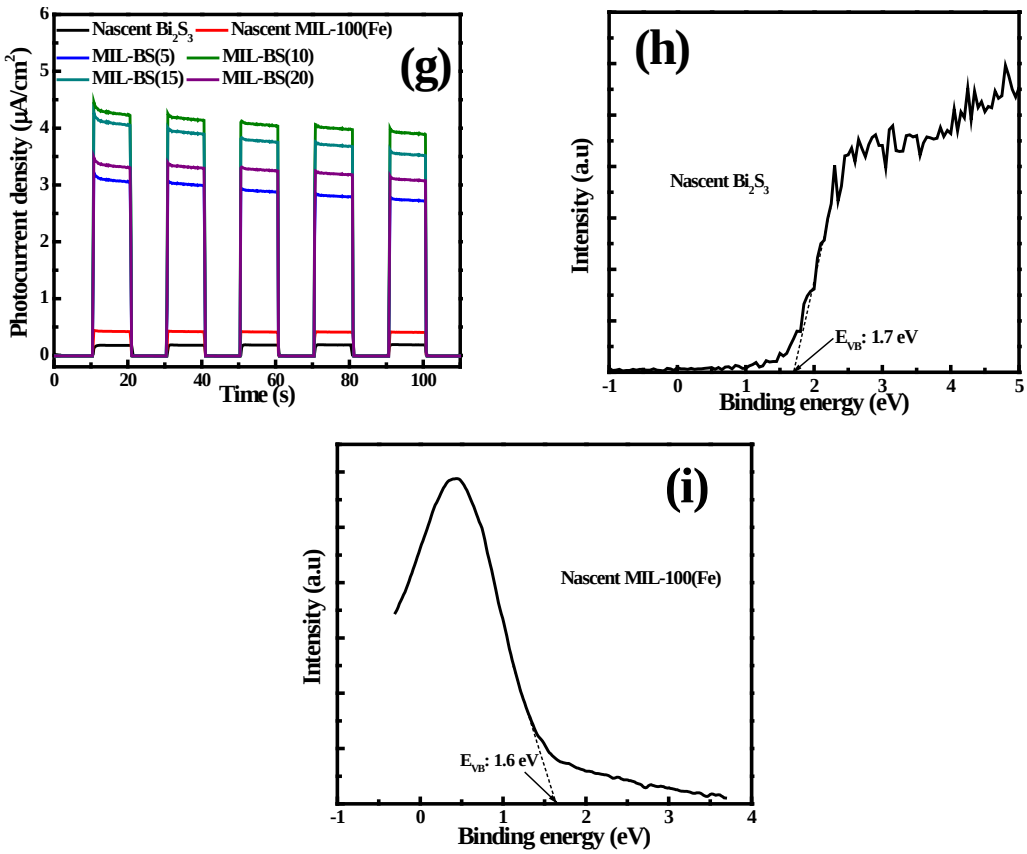

Fig. S2. (a) N_2 adsorption-desorption isotherms of different materials; (b) UV-Vis DRS analysis of various catalysts; (c) Kubelka Munk functional plot of all the catalysts; (d) Zeta potential variation with solution pH for nascent and composite catalysts; (e) PL analysis; (f) Nyquist plots; (g) photocurrent response curves of different single catalysts and binary composites; VB spectrums of (h) nascent Bi_2S_3; (i) nascent MIL-100(Fe).

S3. Catalytic degradation of RhB

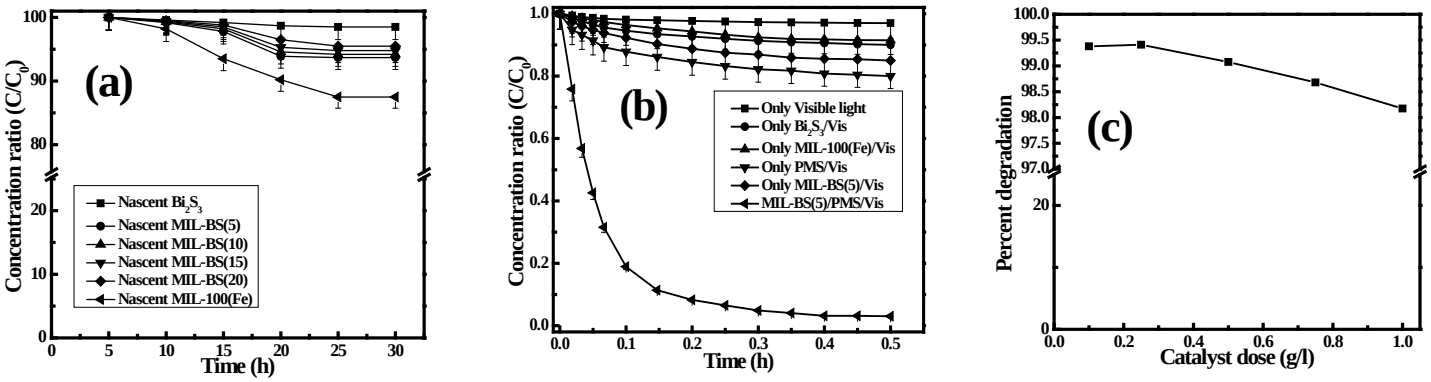

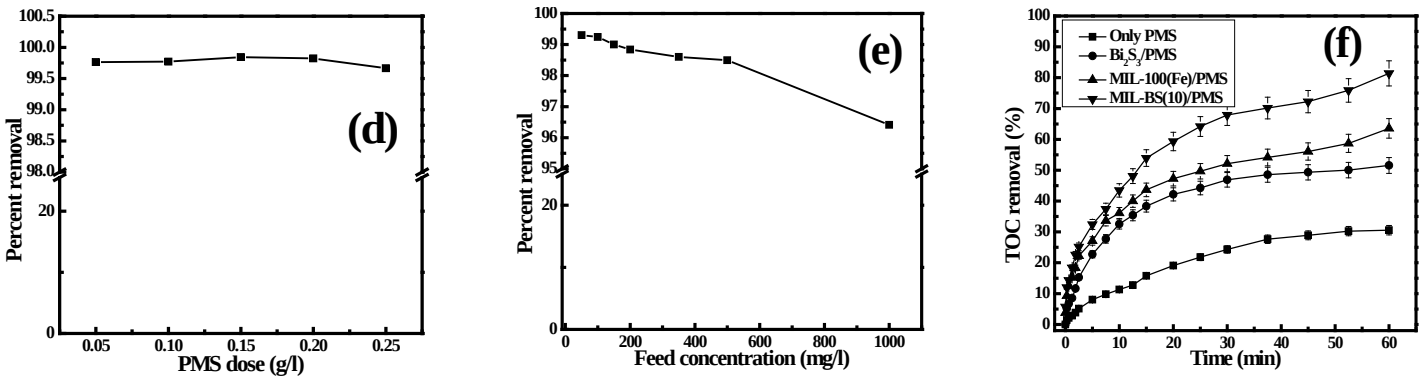

Fig. S3. Temporal variation of residual RhB concentration for (a) adsorption on different nascent primary components and binary composites; (b) different catalyst/PMS/Visible combination; Percent degradation of RhB in medium for alteration of (c) catalyst dose; (d) PMS dose; (e) initial RhB concentration; (f) extent of TOC removal for various catalyst/PMS combination. (Experimental conditions: RhB initial concentration: 100 mg/l, catalyst dose: 0.025 g/l, PMS dose: 0.15 g/l, initial solution pH: 7.0, operating temperature: 308K, visible light intensity: 80W, rotational speed: 150rpm)

S4. Effect of coexisting anions and natural organic matter

The following reactions are involved in the radical quenching process of HCO_3^- anions:

$$HCO_3^-(aq) + SO_4^{\bullet-}(aq) \rightarrow SO_4^{2-}(aq) + CO_3^{\bullet-}(aq) + H^+(aq) \quad (S1)$$

$$HCO_3^-(aq) + OH^{\bullet}(aq) \rightarrow CO_3^{\bullet-}(aq) + H_2O(l) \quad (S2)$$

The following reactions are involved in the scavenging effects of the $H_2PO_4^-$ anions in the reaction medium:

$$H_2PO_4^-(aq) + SO_4^{\bullet-}(aq) \rightarrow SO_4^{2-}(aq) + HPO_4^{\bullet-}(aq) + H^+(aq) \quad (S3)$$

$$H_2PO_4^-(aq) + OH^{\bullet}(aq) \rightarrow HPO_4^{\bullet-}(aq) + H_2O(l) \quad (S4)$$

The following reactions are involved in the scavenging process by the NO_3^- anions

$$NO_3^-(aq) + h+/OH^{\bullet}/SO_4^{\bullet-}(aq) \rightarrow NO_3^{\bullet}(aq) + OH^- / SO_4^{2-}(aq) \quad (S5)$$

$$NO_3^-(aq) + H_2O(l) + e^-(aq) \rightarrow NO_3^{\bullet}(aq) + 2OH^-(aq) \quad (S6)$$

The following reactions are involved in the scavenging process by the SO_4^{2-} anions

$$SO_4^{2-}(aq) + OH^{\bullet}(aq) \rightarrow SO_4^{\bullet-}\left(HSO_4^{\bullet}\right)(aq) + OH^-(aq) \quad (S7)$$

$$2SO_4^{\bullet-}(aq) \rightarrow S_2O_8^{2-}(aq) \quad (S8)$$

$$SO_4^{\bullet-}(aq) + S_2O_8^{2-}(aq) \rightarrow SO_4^{2-}(aq) + S_2O_8^{\bullet-}(aq) \quad (S9)$$

The following reactions are involved in the scavenging process by the Cl^- anions:

$$Cl^-(aq) + HSO_5^-(aq) \rightarrow SO_4^{2-}(aq) + HOCl(aq) \quad (S10)$$

$$2Cl^-(aq) + H^+(aq) + HSO_5^-(aq) \rightarrow SO_4^{2-}(aq) + Cl_2(aq) + H_2O(l) \quad (S11)$$

$$Cl^-(aq) + SO_4^{\bullet-}(aq) \rightarrow Cl^{\bullet}(aq) + SO_4^{2-}(aq) \quad (S12)$$

$$Cl^{\bullet}(aq) + Cl^-(aq) \rightarrow Cl_2^{\bullet-}(aq) \quad (S13)$$

Typical reactions of NOMs with $OH^{\bullet}$ and $SO_4^{\bullet-}$ radicals are given as:

$$NOM(aq) + SO_4^{\bullet-}(aq) \rightarrow \text{Products (aq)} \qquad k = 2.35\times10^7 M^{-1}s^{-1} \quad (S14)$$

$$NOM(aq) + OH^{\bullet}(aq) \rightarrow \text{Products (aq)} \qquad k = 3.0\times10^8 M^{-1}s^{-1} \quad (S15)$$

S5. Reaction mechanism

The reactions involved in the activation of PMS and degradation of RhB are given below [1–3]:

$$HSO_5^-(aq) \rightarrow H^+(aq) + SO_5^{2-}(aq) \quad (S16)$$

$$SO_5^{2-}(aq) + H_2O(l) \rightarrow H^+(aq) + SO_4^{2-}(aq) + O_2^{\bullet-}(aq) \quad (S17)$$

$$2HSO_5^-(aq) \rightarrow SO_4^{\bullet-}(aq) + SO_5^{\bullet-}(aq) + H_2O(l) \quad (S18)$$

$$2HSO_5^-(aq) \rightarrow SO_5^{\bullet-}(aq) + HSO_4^{\bullet-}(aq) + OH^-(aq) \quad (S19)$$

$$2SO_5^{\bullet-}(aq) \rightarrow 2SO_4^{\bullet-}(aq) + O_2(g) \quad (S20)$$

$$Fe^{3+}\big|_{surf.} + O_2^{\bullet-}(aq) \rightarrow Fe^{2+}\big|_{surf.} + O_2(g) \quad (S21)$$

$$Fe^{2+}\big|_{surf.} + HSO_5^-(aq) \rightarrow Fe^{3+}\big|_{surf.} + SO_4^{2-}(aq) + OH^{\bullet}(aq) \quad (S22)$$

$$Fe^{2+}\big|_{surf.} + HSO_5^-(aq) \rightarrow Fe^{3+}\big|_{surf.} + SO_4^{\bullet-}(aq) + OH^-(aq) \quad (S23)$$

$$Fe^{3+}\big|_{surf.} + HSO_5^-(aq) \rightarrow Fe^{2+}\big|_{surf.} + SO_5^{\bullet-}(aq) + H^+(aq) \quad (S24)$$

$$Fe^{2+}/Fe^{3+}\big|_{surf.}\text{---}(OH) + HSO_5^-(aq) \rightarrow Fe^{2+}/Fe^{3+}\big|_{surf.}\text{---}(OH)(OSO_3^-) + OH^-(aq) \quad (S25)$$

$$Fe^{2+}/Fe^{3+}\big|_{surf.}\text{---}(OH)(OSO_3^-) \rightarrow Fe^{3+}/Fe^{2+}\big|_{surf.}\text{---}(OH) + SO_4^{\bullet-}(aq) \quad (S26)$$

$$Fe^{3+}\big|_{surf.}\text{---}(OH) \rightarrow Fe^{2+}\big|_{surf.}\text{---}(O^{\bullet})(OSO_3^-) + H_2O(l) \quad (S27)$$

$$2\,Fe^{2+}\big|_{surf.}\text{---}(O^{\bullet})(OSO_3^-) + 2H_2O(l) \rightarrow 2\,Fe^{2+}\big|_{surf.}\text{---}(OH) + O_2(g) + 2SO_4^{\bullet-}(aq) \quad (S28)$$

$$Bi^{3+}\big|_{surf.} + Fe^{3+}\big|_{surf.} \rightarrow Bi^{4+}\big|_{surf.} + Fe^{2+}\big|_{surf.} \quad (S29)$$

$$Bi^{3+}\big|_{surf.}\text{--}S_{surf.}^{2-} + H^+(aq) \rightarrow Bi^{4+}\big|_{surf.} + H_2S(g) \quad (S30)$$

$$Bi^{3+}\big|_{surf.} + HSO_5^-(aq) \rightarrow Bi^{4+}\big|_{surf.} + SO_4^{\bullet-}(aq) + OH^-(aq) \quad (S31)$$

$$Bi^{4+}\big|_{surf.} + HSO_5^-(aq) \rightarrow Bi^{3+}\big|_{surf.} + SO_5^{\bullet-}(aq) + H^+(aq) \quad (S32)$$

$$Bi^{3+}/Bi^{4+}\Big|_{surf.}\text{---(OH)}+HSO_5^-(aq) \rightarrow Bi^{3+}/Bi^{4+}\Big|_{surf.}\text{---(OH)}(OSO_3^-)+OH^-(aq) \quad \text{(S33)}$$

$$Bi^{4+}/Bi^{3+}\Big|_{surf.}\text{---(OH)}(OSO_3^-) \rightarrow Bi^{3+}/Bi^{4+}\Big|_{surf.}\text{---(OH)}+SO_4^{\bullet-}(aq) \quad \text{(S34)}$$

$$HSO_5^-(aq)+SO_5^{2-}(aq) \rightarrow SO_4^{2-}(aq)+HSO_4^{\bullet-}(aq)+O_2^1(aq) \quad \text{(S35)}$$

$$O_2^{\bullet-}(aq)+OH^{\bullet}(aq) \rightarrow OH^-(aq)+O_2^1(aq) \quad \text{(S36)}$$

$$2O_2^{\bullet-}(aq)+2H_2O(l) \rightarrow 2O_2^1(aq)+2OH^-(aq)+H_2O_2(aq) \quad \text{(S37)}$$

$$RhB(aq)+h\nu \rightarrow RhB^*(aq) \rightarrow RhB^{*+}(aq)+e^-(aq) \quad \text{(S38)}$$

$$RhB^{*+}(aq)+\left(OH^{\bullet}/SO_4^{\bullet-}/O_2^{\bullet-}/O_2^1\right)(aq) \rightarrow \text{intermediates}(aq) \rightarrow CO_2(g)+H_2O(l) \quad \text{(S39)}$$

S6. RhB degradation pathway

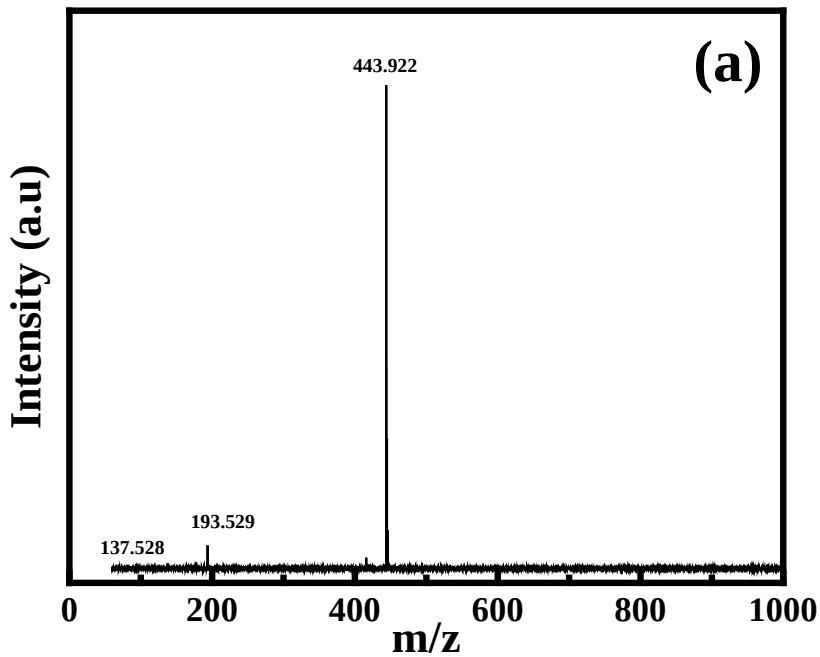

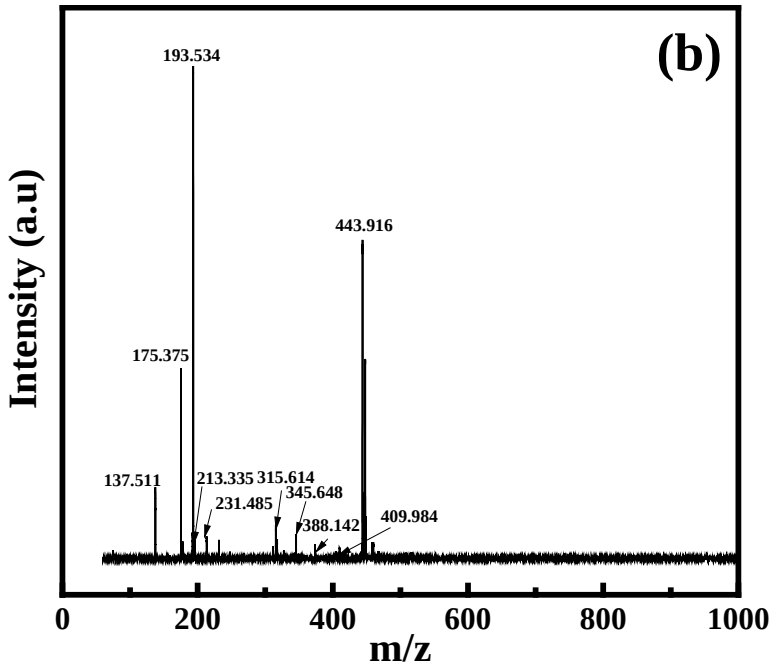
(b)
Intensity (a.u)
193.534
443.916
175.375
137.511
213.335
315.614
231.485
345.648
388.142
409.984
0
200
400
600
800
1000
m/z

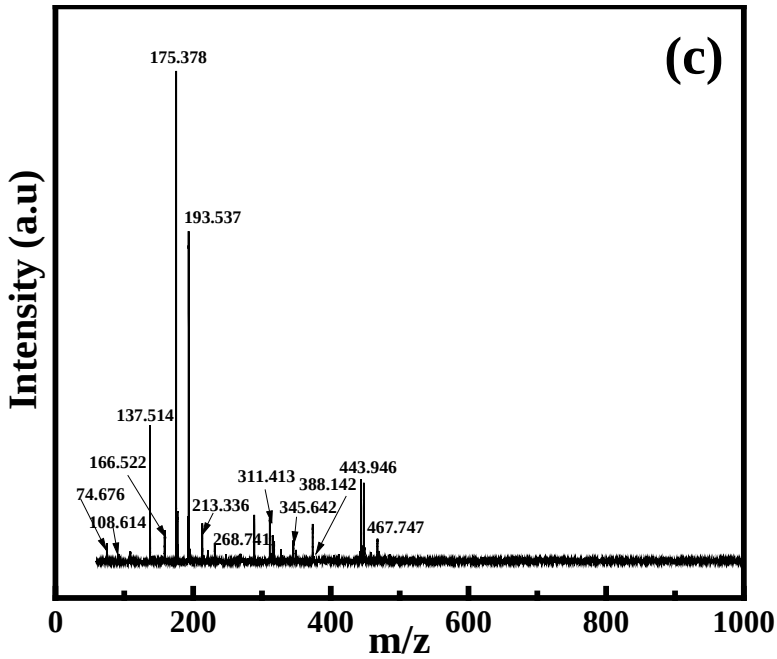
(c)
Intensity (a.u)
175.378
193.537
137.514
166.522
74.676
108.614
213.336
268.741
311.413
345.642
388.142
443.946
467.747
0
200
400
600
800
1000
m/z

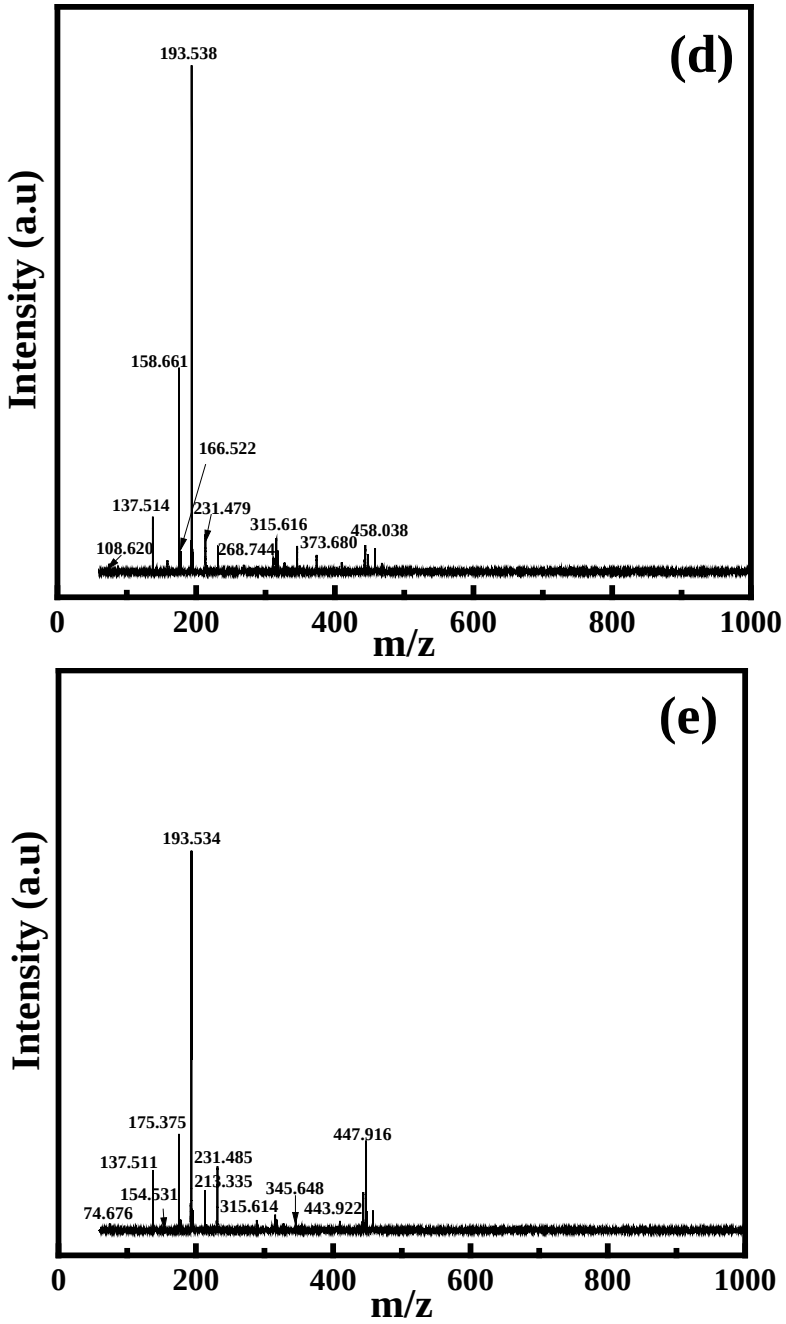

Fig. S4. MALDI-TOF/TOF mass spectra for (a) RhB Feed; photodegraded solution after (b) 5 min; (c) 10 min; (d) 15 min; (e) 20 min

Table S2. Degradation intermediates and corresponding details

Intermediate serial no.	Chemical name and abbreviations	Molecular weight	Chemical formula

I_1	Rhodamine B (RhB)	443	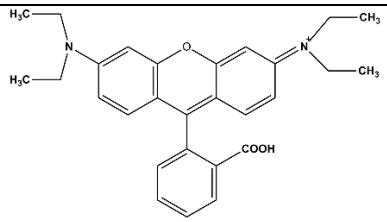
$I_{2(1)}$	Hydroxylated Rhodamine B (OH-RhB)	459	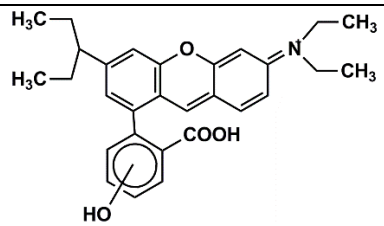
$I_{2(2)}$	Hydroxylated Rhodamine B (OH-RhB)	459	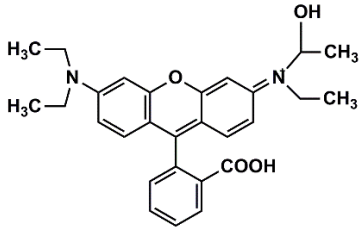
I_3	N,N-diethyl-N'-ethyl rhodamine (DER)	415	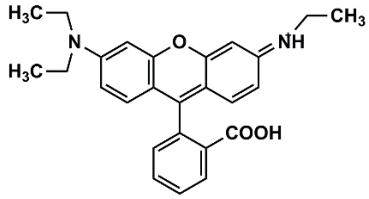
I_4	N,N-diethyl rhodamine (DR)	388	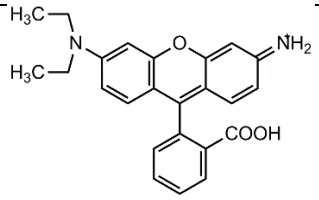
I_5	N-ethyl-N'-ethyl rhodamine (EER)	388	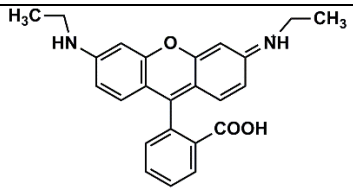
I_6	N-ethyl rhodamine (ER)	360	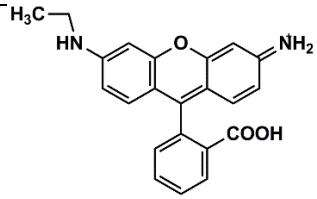
I_7	Rhodamine (R)	332	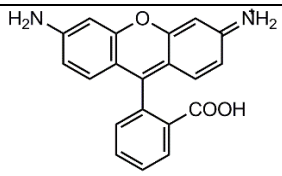

I_8	Amino rhodamine	317	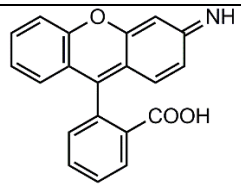
I_9	2-(3H-xanthen-9-yl) benzoic acid	302	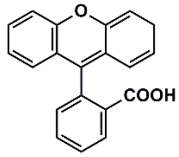
I_{10}	9-phenyl-3H-xanthene	257	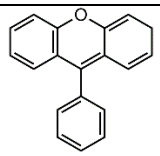
I_{11}	benzoic acid	123	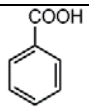
I_{12}	Diphenol	110	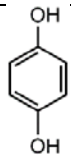
I_{13}	Phenol	94	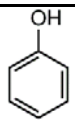
I_{14}	Benzaldehyde	106	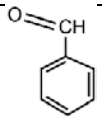
I_{15}	adipic acid	146	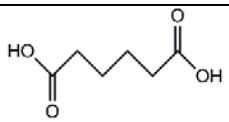
I_{16}	phthalic acid	166	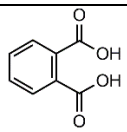
I_{17}	isophthalic acid	166	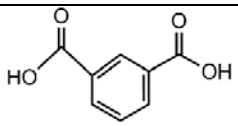
I_{18}	terephthalic acid	166	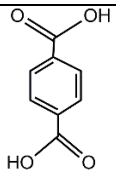
I_{19}	2,4,6-trihydroxybenzoic acid	170	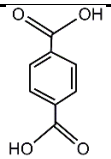

I_{20}	4-hydroxy benzoic acid	138	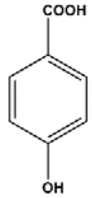
I_{21}	2,4-dihydroxy benzoic acid	154	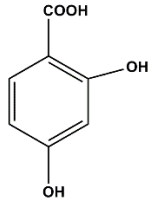
I_{22}	2,4,6-trihydroxy benzoic acid	172	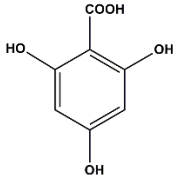

Table S3. Comparative analysis of the synthesized catalyst (MIL-BS)

Sl. no.	Material	Catalyst dose	PMS dose	RhB concentration	Solution pH	Reaction time	Degradation extent	Synthesis of catalyst	Reaction rate constant	Reference
1	Oxygen vacancy rich CuO	0.3 g/L	0.12 g/L	20 mg/L	7	20 mins	98%	Citrate assisted precipitation method		4
2	N-doped Cu/Fe@PC from MOF	0.1 g/L	0.2 g/L	50 mg/L	4.5	30 mins	100%	One step pyrolysis of gCN doped Cu/Fe MOF	0.5307 min^{-1}	5
3	$BiVO_4$ nanostrcutured films	Thin film	0.06 g/L	12 mg/L	7	20 mins	100%	thermal reaction between electrodeposited Bi films and V precursor	0.175 min^{-1}	6
4	Highly dispersed Fe species supported on activated carbon (CA-Fe-C)	0.15 g/L	1.0 g/L	100 mg/L	4.1	30 mins	96%	Citric acid assisted ultrasonic pyrolysis method	0.09045 min^{-1}	7
5	Pyrite/Hydroxylamine (HA)	catalyst: 0.4 g/L	0.25 g/L	50 mg/L	4	30 mins	99.30%	Commercially purchased		8
6	Hierarchical porous Fe_3O_4/Co_3S_4	0.05 g/L	0.15 g/L	200 mg/L	6.5	20 mins	100%	Single phase change reaction with heating under inert gas	0.236 min^{-1}	9
7	Fe_3O_4/CoFeCu-LDHs	0.2 g/L	0.15 g/L	50 mg/L	7	20 mins	100%	Coprecipitation method	0.462 min^{-1}	10

8	Co/NCNT	0.02 g/L	0.06 g/L	20 mg/L	5.67	10 mins	99%	One-pot pyrolysis method	1.561 min^{-1}	11
9	Co_3O_4-rice husk ash composites	0.1 g/L	0.5 g/L	20 mg/L	6	60 mins	96.30%	Hydrothermal method	0.18 min^{-1}	12
10	$CoFe_2O_4$/Ag-fMWCNT hybrid	0.2 g/L	1 g/L	20 mg/L	6.5	15 mins	100%	Calcination at 200°C for 12 h	0.331 min^{-1}	13
11	Cobalt sulfide-reduced graphene oxide (CoS-rGO)	0.25 g/L	0.08 g/L	15 mg/L	5	10 mins	99%	Solvothermal method	0.5 min^{-1}	14
12	cPVC/Bi_2O_3	0.33 g/L	0.61 g/L	200 mg/L	7	150 mins	100%	Mixing in aqueous medium, followed by drying	1.21×10^{-4} min^{-1}	15
13	$CoFe_2O_4$@NPC	0.06 g/L	0.3 g/L	100 mg/L	6	20 mins	99%	Insitu growth of MOF, followed by one-step calcination	0.0766 L/mg. min	16
14	SBA-15 mesoporous molecular sieve	0.1 g/L	0.05 g/L	50 mg/L	7	45 mins	99%	Acid-treatment, extraction, crystallization and metal loading	0.169 min^{-1}	17
15	$Co_{1+x}Fe_{2-x}O_4$	0.2 g/L	0.2 g/L	40 mg/L	5	30 mins	100%	Calcination of MOFs at 450°C for 1 h	0.26 min^{-1}	18
16	MIL-100(Fe)/Bi_2S_3	0.025 g/L	0.1 g/L	100 mg/L	7	30 mins	100%	Hydrothermal growth of Bi_2S_3 on dispersed MIL-100(Fe)	4.56 min^{-1}	This work

S7. References

1 H. Zhang, X. Liu, J. Ma, C. Lin, C. Qi, X. Li, Z. Zhou and G. Fan, *J. Hazard. Mater.*, 2018, **344**, 1220–1228.

2 J. M. Dangwang Dikdim, Y. Gong, G. B. Noumi, J. M. Sieliechi, X. Zhao, N. Ma, M. Yang and J. B. Tchatchueng, *Chemosphere*, 2019, **217**, 833–842.

3 J. Wang and S. Wang, *Chem. Eng. J.*, 2018, 334, 1502–1517.

4 Y. Liu, Q. Lan, S. Sun and Q. Yang, *RSC Adv.*, 2022, **12**, 2928–2937.

5 P. Liu, D. Zhong, Y. Xu and N. Zhong, *J. Environ. Chem. Eng.*, 2022, **10**, 107595.

6 K. Missaoui, R. Ouertani, E. Jbira, R. Boukherroub and B. Bessaïs, *Environ. Sci. Pollut. Res.*, 2021, **28**, 52236–52246.

7 Y. Wu, L.-H. Kong, R.-F. Shen, X.-J. Guo, W.-T. Ge, W.-J. Zhang, Z.-Y. Dong, X. Yan, Y. Chen and W.-Z. Lang, *J. Environ. Chem. Eng.*, 2022, **10**, 107463.

8 G.-J. He, D.-J. Zhong, Y.-L. Xu, P. Liu, S.-J. Zeng and S. Wang, *Water, Air, Soil Pollut.*, 2021, **232**, 141.

9 X. Shi, P. Hong, H. Huang, D. Yang, K. Zhang, J. He, Y. Li, Z. Wu, C. Xie, J. Liu and L. Kong, *J. Colloid Interface Sci.*, 2022, **610**, 751–765.

10 T. Li, X. Du, J. Deng, K. Qi, J. Zhang, L. Gao and X. Yue, *J. Environ. Sci.*, 2021, **108**, 188–200.

11 J. Cheng, N. Wei, Y. Wang, Y. Long and G. Fan, *Sep. Purif. Technol.*, 2021, **277**, 119441.

12 J. Di, R. Jamakanga, Q. Chen, J. Li, X. Gai, Y. Li, R. Yang and Q. Ma, *Sci. Total Environ.*, 2021, **784**, 147258.

13 M. O. Abdel-Salam and T. Yoon, *Environ. Res.*, 2022, **205**, 112424.

14 L. Amirache, F. Barka-Bouaifel, P. Borthakur, M. R. Das, H. Ahouari, H. Vezin, A. Barras, B. Ouddane, S. Szunerits and R. Boukherroub, *J. Environ. Chem. Eng.*, 2021, **9**, 106018.

15 H.-H. Pham, S.-J. You, Y.-F. Wang, M. T. Cao and V.-V. Pham, *Sustain. Chem. Pharm.*, 2021, **19**, 100367.

16 Y. Liang, L. Li, C. Yang, L. Ma, W. Mao and H. Yu, *J. Alloys Compd.*, 2022, **907**, 164504.

17 Y. Xu, E. Hu, D. Xu and Q. Guo, *Sep. Purif. Technol.*, 2021, **274**, 119081.

18 J. Zhao, H. Wei, P. Liu, A. Zhou, X. Lin and J. Zhai, *J. Environ. Chem. Eng.*, 2021, **9**, 105412.